Ischemic renal injury reveals in vivo functions for the von Hippel-Lindau tumor suppressor in mitotic fidelity control

Hell, Michael P ; Duda, Maria ; Weber, Thomas C ; Moch, Holger ; Krek, Wilhelm

Abstract: The von Hippel-Lindau (VHL) tumor suppressor protein pVHL is commonly mutated in clear cell renal cell carcinoma (ccRCC) and has been implicated in the control of multiple cellular processes that might be linked to tumor suppression including promoting proper spindle orientation and chromosomal stability. However, it is unclear whether pVHL exerts these mitotic regulatory functions also in vivo. Here we applied ischemic kidney injury to stimulate cell division in otherwise quiescent mouse adult kidneys. We show that in the short-term (5.5 days post surgery), Vhl-deficient kidney cells demonstrate both spindle misorientation and aneuploidy. The spindle misorientation phenotype encompassed changes in directed cell division, which may manifest in the development of cystic lesions, while the aneuploidy phenotype involved the occurrence of lagging chromosomes but no chromosome bridges indicative of mitotic checkpoint impairment. Intriguingly, in the long-term (four months after the ischemic insult), Vhl-deficient kidneys displayed a heterogeneous pattern of ccRCC precursor lesions including cysts, clear cell-type cells, and dysplasia. Together, these data provide direct evidence for a key role of pVHL in mediating oriented cell division and faithful mitotic checkpoint function in the renal epithelium, emphasizing the importance of pVHL as a controller of mitotic fidelity in vivo.

DOI: https://doi.org/10.1158/0008-5472.CAN-13-2040

Cancer Research

Ischemic renal injury reveals in vivo functions for the von Hippel-Lindau tumor suppressor in mitotic fidelity control

Michael P Hell, Maria Duda, Thomas C Weber, et al.

Cancer Res Published OnlineFirst December 20, 2013.

Tumor suppressor VHL functions in the control of mitotic fidelity

Michael P. Hell[1,4], Maria Duda[1,4], Thomas C. Weber[2], Holger Moch[3], and Wilhelm Krek[1,5]

[1] *Institute of Molecular Health Science, ETH Zurich, Schafmattstr. 22, 8093 Zurich, Switzerland*

[2] *Rodent Center HCI, ETH Zurich, Wolfgang-Pauli-Str. 10, 8093 Zurich, Switzerland*

[3] *Institute of Surgical Pathology, University Hospital Zurich, Schmelzbergstrasse 12, 8091 Zurich, Switzerland*

[4] These authors contributed equally

[5] Corresponding author: Email: wilhelm.krek@biol.ethz.ch

Tel: +41 44 633 34 47

No potential conflict of interest

Running title: VHL suppresses spindle misorientation and aneuploidy *in vivo*.

Keywords: ischemic kidney injury, spindle misorientation, aneuploidy, Vhl, renal cancer

Precis: This study reveals a function for the von Hippel-Lindau protein in spatially oriented cell division and faithful mitotic checkpoint function in the renal epithelium, where this tumor suppressor has a pivotal role in blocking tumorigenesis.

Abstract

The von Hippel-Lindau (*VHL*) tumor suppressor protein pVHL is commonly mutated in clear cell renal cell carcinoma (ccRCC) and has been implicated in the control of multiple cellular processes that might be linked to tumor suppression including promoting proper spindle orientation and chromosomal stability. However, it is unclear whether pVHL exerts these mitotic regulatory functions also *in vivo*. Here we applied ischemic kidney injury to stimulate cell division in otherwise quiescent mouse adult kidneys. We show that in the short-term (5.5 days post surgery), *Vhl*-deficient kidney cells demonstrate both spindle misorientation and aneuploidy. The spindle misorientation phenotype encompassed changes in directed cell division, which may manifest in the development of cystic lesions, while the aneuploidy phenotype involved the occurrence of lagging chromosomes but no chromosome bridges indicative of mitotic checkpoint impairment. Intriguingly, in the long-term (four months after the ischemic insult), *Vhl*-deficient kidneys displayed a heterogeneous pattern of ccRCC precursor lesions including cysts, clear cell-type cells, and dysplasia. Together, these data provide direct evidence for a key role of pVHL in mediating oriented cell division and faithful mitotic checkpoint function in the renal epithelium, emphasizing the importance of pVHL as a controller of mitotic fidelity *in vivo*.

Introduction

Inactivation of the *VHL* tumor suppressor gene plays a causal role in the development of hereditary (von Hippel-Lindau disease) and sporadic clear cell carcinoma of the kidney, establishing *VHL* as a critical 'gatekeeper' of the renal epithelium (1). The gene product of *VHL*, pVHL, is a multifunctional protein implicated in the regulation of a variety of cellular processes essential for epithelial homeostasis including cell growth and differentation, modulation of cell death pathways, extracellular matrix deposition, hypoxia response and primary cilium maintenance (2, 3).

Recent cell-based studies in *VHL*-deficient renal carcinoma cell lines unveiled a critical role for pVHL in the regulation of two key aspects of mitosis – suppression of spindle misorientation and preservation of normal mitotic checkpoint function (4). Spindle misorientation has been linked, in this setting, to unstable astral microtubules, while impaired mitotic checkpoint function and resultant aneuploidy involves a mechanism causing reduced expression of Mad2, a spindle checkpoint control protein, whose changes in abundance is associated with impaired mitotic checkpoint function.

Whether these newly identified mitotic functions of pVHL are relevant *in vivo* in the renal epithelium is not known. However, both of these mitotic functions could potentially contribute to key characteristics of human *VHL*-associated pathology (1, 5, 6). In the renal epithelium, changes in spindle orientation could, in principle, alter the directionality of cell division a phenomenon believed to contribute to cyst formation during development (7, 8). Similarly, the production of chromosome missegregation errors could culminate in the emergence of aneuploid cells, a well-known enabling feature of tumor

development (9, 10). To test this directly, we resorted to an injury-regeneration model, wherein kidney epithelial cells are challenged with ischemic injury and are consequently induced to re-enter the cell cycle as part of a regenerative response of the tissue (11, 12). Our cell biological and molecular analyses of primary mouse renal epithelial cells and kidney epithelia from kidney-specific *Vhl*-deficient and Cre-negative control mice that have been challenged with ischemic injury, highlight a key role for *Vhl* as a suppressor of spindle misorientation and chromosomal instability *in vivo*.

Materials & methods

Mouse strain information and general techniques

Kidney specific *Vhl* knockout mice ($Vhl^{\Delta/\Delta}$) were obtained as described previously (13, 14). Mice were kept under standard pathogen free conditions in accordance with Swiss animal welfare regulations.

Ischemic kidney injury surgery

Kidney clamp surgery was performed under sterile conditions in a laminar flow hood on 6-9 week old female mice. Anesthesia was initiated with 5 vol.% isoflurane in pure oxygen (800 mL/min) and maintained at approx. 2 vol.% isoflurane (500 mL/min O_2). Additionally, a single dose of buprenorphine (0.2 mg/kg, s.c.) was given. To initiate the injury, a non-traumatic micro aneurysm clip (Harvard apparatus, #610186) was placed around the left renal pedicle for 30 minutes, followed by reperfusion after clamp removal. The right kidney remained unclamped and served as internal control. Animals were

sacrificed 5.5 days or 4 months post injury and both kidneys were removed for further analysis. In the case of long-term experiment, one animal per surgery session was included that was sacrificed already after 5.5 days to confirm the efficiency of the kidney clamp.

Primary kidney cell preparation and culturing

Kidneys were dissected from 6-7 week old $Vhl^{fl/fl}$ male mice, and further processed under sterile conditions as described previously (15). Kidneys were cut into small pieces with a surgical razorblade and digested at 37°C for 30 minutes with collagenase 4a (200 U/mL, Worthington Biochemical Corp., NJ, U.S.A.). Digested tissue was passed through a 70 µm cell strainer and washed with 5% fetal calf serum (FCS) in PBS. Cells were re-suspended and plated in K-1 medium [Dulbecco's modified Eagle's medium (50:50 mixture of DMEM and Ham`s F12), supplemented with 2.5% FCS (Bioconcept), 5% horse serum (Bioconcept), 10 mM Hepes (Life Technologies), 1.1 mg/mL sodium bicarbonate (Sigma), 5 µg/mL insulin (Sigma), 25 ng/mL prostaglandin E_1 (PGE_1) (Sigma), 5 x 10^{-12} M triiodothyronine (Sigma), 10 nM sodium selenite (Sigma), 5 x 10^{-8} M hydrocortisone, and 5 µg/mL transferrin (Sigma)]. Seven days post-plating, cells were infected with adenovirus expressing Cre or Cre-IRES-GFP and LacZ or GFP as control, respectively, and optionally with pLKO lentivirus overexpressing pVHL or a control cassette (R. Pawłowski, A. Ittner, unpublished) and selected for 3 days on puromycin (2 µg/mL) prior to harvesting for subsequent assays.

Western blotting

Western blot was performed as described previously (4). The following antibodies were used in this study: anti-mouse pVHL(m)CT antibody (16) and anti-Cdk2 (Santa Cruz Biotechnologies, sc-163-G).

Transcription Analyses

RNA was isolated from cultured cells of equal confluency using TRIzol (Life Technologies) according to the manufacturer's instructions. One µg of total RNA was reversely transcribed using a premixed polymerase mix (EcoDry, Clontech) and analyzed by quantitative realtime PCR (qPCR) using the SYBR Green system on a LightCycler (Roche Applied Science) instrument. The following primer pairs were used (all yielding PCR products with a single melting point): Glut1: 5'-CAG TTC GGC TAT AAC ACT GGT G-3' and 5'-GCC CCC GAC AGA GAA GAT G-3', PGK1: 5'-TGG AGC CAA CTC CGT TGT C-3' and 5'- CAG GCA TTC TCG ACT TCT GGG-3', VEGFA: 5'-CTT GTT CAG AGC GGA GAA AGC-3' and 5'-ACA TCT GCA AGT ACG TTC GTT-3', HPRT: 5'-TCA GTC AAC GGG GGA CAT AAA-3' and 5'-GGG GCT GTA CTG CTT AAC CAG-3'.

Staining methods

Cells grown on a coverslip were fixed for 5 min with cold methanol. Kidneys were cut in half and fixed overnight either with 4% PFA or formalin. PFA-fixed tissues were embedded in 4% low-melting point (LMP) agarose (W5376R, Fischer Scientific) prior to cutting (50 µm sections) with a vibratome (Hyrax

V50, Zeiss). Formalin-fixed tissues were dehydrated on a TPC 15 Duo (MediteAG) tissue processor and subsequently treated in a paraffin embedding station (MediteAG). Sections (4 or 10 µm) were cut on a HM 355S microtome with Cool Cut and Section-Transfer-System STS (Microm AG). The following primary antibodies were used: anti□α−tubulin (homemade from rat hybridoma clone YL1/2. Sigma-Aldrich, St. Louis), anti-phoshorylated (Ser10) histone 3 (p-H3, Cell Signaling, 9706S), anti Ki-67 (Dako Cytomation, M7249), anti thiazide-sensitive sodium chloride cotransporter NCC (Millipore, AB3553), anti-glucose transporter 1, (Glut1, abcam, ab14683), anti hypoxia-inducible factor 1 alpha (HIF1α, Novus Biologicals NB100-479), anti-gamma tubulin (Sigma, t3559 and Abcam, ab11316), anti E-cadherin (Cell Signaling, 3195S, clone 24E10), anti atypical protein kinase C zeta (aPKCz, Santa Cruz, sc-17781). All secondary antibodies were obtained from LifeTechnologies. Rhodamine labeled *Dolichos Biflorus* Agglutinin (DBA, Vector Laboratories Inc. RL-1032) was used for direct labeling of distal tubules (as a replacement of NCC in case of species cross-reactivity). DAPI (4',6-diamidino-2-phenylindole) was applied as nuclear counterstain. Hematoxylin and eosin (H&E) stainings were performed on an automatic COT 20 stainer (Medite AG). Terminal deoxynucleotidyl transferase dUTP nick end labeling (TUNEL) was performed using the in-situ cell death detection kit (Roche Applied Sciences) according to the manufacturer's protocol. Fluorescence in-situ hybridization (FISH) detection of murine chromosome 7 was performed after antigen retrieval and protein digestion (45 minutes, Digest-All III, LifeTechnologies) with a probe provided by Heather Flynn Gilmer and Dr. Patricia T. Greipp (Mayo Clinics, Cleveland, U.S.A., see also (17)).

Image acquisition was performed on widefield (Zeiss Axioplan2 and Observer Z2, DeltaVision personalDV) and confocal (Zeiss LSM510 or Leica TCS SP2) fluorescence microscopes. Chromogenic stains were analyzed on a Zeiss AxioImager A1. Image analysis was performed using ImageJ (National Institutes of Health, U.S.A.), Imaris (Bitplane, AG), and the ZEN software (Zeiss).

Metaphase Spreads

Exponentially growing cells were arrested in metaphase using nocodazole (250 ng/mL, overnight treatment). Cells were collected and treated for 7 minutes in buffered hypotonic solution (0.05 M KCl, 0.02 M Tris pH 7.5). Subsequent fixation was performed with pre-chilled methanol/acetic acid (3:1) at ambient temperature for 10 min. Metaphase spreads were performed by dropping cell suspension at 37°C in a humidified environment and mounted in mowiol (Calbiochem) containing 1 µg/mL DAPI (4',6-diamidino-2-phenylindole).

Spindle angle measurements

Spindle angle measurements were performed as described elsewhere (8). Shortly, Z-stack images were acquired (0.5 µm for kidney sections, 0.3 µm for primary kidney cells) and the three-dimensional representation of the image was done using Imaris software (Bitplane, AG). Only sections with a complete mitotic spindle were included in the further analysis. The three-dimensional coordinates describing the direction of the kidney tubule and the mitotic

spindle were used to calculate the net angle of division. In case of cross sections, the z-dimension was omitted as not relevant for the type of analysis. The following mathematical formulas where used:

Net angle: $$\cos\alpha = \frac{a \bullet b}{|a| * |b|} = \frac{a_x b_x + a_y b_y + a_z b_z}{\sqrt{a_x{}^2 + a_y{}^2 + a_z{}^2} * \sqrt{b_x{}^2 + b_y{}^2 + b_z{}^2}}$$

Cross-section angle: $$\cos\alpha = \frac{a \bullet b}{|a| * |b|} = \frac{a_x b_x + a_y b_y}{\sqrt{a_x{}^2 + a_y{}^2} * \sqrt{b_x{}^2 + b_y{}^2}}$$

Statistics and Error Analysis

Data is plotted as mean ± standard deviation, mean ± SEM, or median (indicated in the figure legend). If applicable, Gaussian error propagation was utilized. In cases where normal distribution could be assumed, a two-sided unpaired Student's *t*-test was applied; otherwise the Mann-Whitney U test was employed. P-values: * $p < 0.05$, ** $p < 0.01$, *** $p < 0.001$. For the sake of clarity, non-significant associations were only mentioned when instructive. Significant changes in chromosome number distribution were tested for by using Mood's test (18) in the statistical package R (19). Differences in the frequency of lagging chromosome (single or multiple combined vs. normal and chromosome bridges) as well as chromosome FISH counts were assessed with the Chi-squared (χ^2) test.

Results

Loss of *Vhl* in primary mouse renal epithelial cells *in vitro* induces spindle misorientation and aneuploidy

To assess the influence of *Vhl* loss-of-function on spindle misorientation and aneuploidy generation in the context of mouse primary renal epithelial cells (MRECs), we isolated renal epithelial tubule cells from mice homozygously carrying loxP-flanked *Vhl* alleles ($Vhl^{fl/fl}$) and genetically inactivated *Vhl* by adenoviral transduction with Cre-recombinase (AdCre). As a control, the same cells were infected with an adenovirus expressing LacZ (AdLacZ). Immunoblotting confirmed the successful excision of *Vhl* (Fig. 1A). Using immunofluorescence microscopy, we analyzed spindle assembly checkpoint-dependent and -independent chromosome segregation errors that include in particular lagging chromosomes and chromosome bridges, respectively (Fig. 1B). Quantification of these images revealed an increased occurrence of single and multiple lagging chromosomes, while the rate of chromosome bridges remained unchanged (Fig. 1C), indicative of a weakened spindle checkpoint. To further corroborate this finding, we counted the number of chromosomes in metaphase spreads prepared from wildtype and *Vhl*-deficient MRECs. As illustrated in Fig. 1D, the distribution of chromosome numbers in *Vhl*-deleted cells is significantly broader than in the corresponding *Vhl*-positive MRECs, suggestive of increased levels of aneuploidy.

In parallel, we investigated whether ablation of *Vhl* also leads to spindle misorientation in MRECs. As a measure of misorientation we determined the spindle angle, defined by the direction of the spindle relative to the glass support (Fig. 1E). While the mitotic spindles in AdLacZ-treated cells

preferentially aligned parallel to the support, inactivation of pVHL caused the spindle to be more frequently tilted (Fig. 1F). Quantification of the spindle angle showed a siginificant increase of the median spindle angle in *Vhl*$^{-/-}$ cells compared to control cells (Fig. 1G). At the same time, the spindle diameter remained unaffected (Fig. 1H).

To independently confirm the pVHL-specificity, we performed a rescue experiment where we reexpressed full-length pVHL in *Vhl*$^{fl/fl}$ MRECs transduced with AdGFP or AdCre (co-expressing GFP). GFP-positivity combined with immunofluorescence stainings for hypoxia-inducible factor 1 alpha (HIF1α), which is stabilized upon pVHL-depletion, provided us with a single cell-based readout for absence or presence of pVHL (Supplemental Fig. 1 A, B). Assessment of mRNA levels of HIF1α target genes confirmed also that *Vhl* was successfully deleted or reexpressed (Supplemental Fig. 1C). As shown in Supplemental Fig. 1D and 1E, we could recapitulate that loss of *Vhl* introduces chromosome missegregation and spindle misorientation, while reexpression of full-length pVHL rescued these phenotypes, consistent with the view that suppression of these phenomena are part of the proposed 'gate-keeper' function of pVHL in kidney epithelial cells.

Analysis of proliferative and apoptotic response of *Vhl*-deficient kidney cells *in vivo* following renal injury

Next we applied an ischemic injury model to kidney-specific *Vhl* knockout mice (*Vhl*$^{\Delta/\Delta}$) and Cre-negative littermates. In this model, kidney epithelial cells are encouraged to re-enter the cell cycle as part of a regenerative

response of the tissue. To this end, we subjected mice to unilateral clamping of the left kidney pedicle before kidney reperfusion. The right kidney remained unstressed and served as internal control. Both kidneys were harvested at 5.5 days post-surgery (Fig. 2A), as at this time point we observed maximal injury-induced kidney cell proliferation. Kidney weight did not significantly change between either clamped and the corresponding contralateral control kidney or Cre- and $Vhl^{\Delta/\Delta}$ littermates (Fig. 2B). Macroscopcially, the clamped kidney appeared slightly paler (Supplemental Fig. 2A). We did not observe any differences in the extend of clamping-induced injury after 5.5 days between clamped Cre-negative and $Vhl^{\Delta/\Delta}$ kidneys (Supplemental Fig. 2B). Additionally, in each case, as demonstrated in Supplemental Figs. 3A, B, we reconfirmed the pVHL status by specific immunostainings for HIF1α and glucose transporter 1 (Glut1), which are well-established readouts for *Vhl*-negativity (20, 21).

To provide evidence that induction of proliferation had occurred, we immunofluorescently stained kidney tissue with antibodies recognizing the proliferation marker Ki-67, and phosphorylated histone 3 (p-H3) to label mitotic cells. Upon injury, we observed a dramatic increase in staining for both Ki-67 and p-H3 in clamped kidneys compared to unstressed control kidneys (Supplemental Fig. 3C). In addition, the observed high rates of proliferation were accompanied by enhanced apoptosis, as evidenced by increased TUNEL positivity in injured compared to control kidneys (Supplemental Fig. 3D). Kidney-specific *Vhl* deletion did not measurably affect neither the proliferative nor the apoptotic response compared to Cre-negative kidneys

(Fig. 2C-G). Thus, *Vhl*-deficiency does not affect to any noticeable degree the proliferative and apoptotic responses of kidneys to ischemic injury.

pVHL suppresses spindle misorientation in kidney tubule cells *in vivo*

To assess whether mitotic spindle orientation is perturbed in $Vhl^{\Delta/\Delta}$ kidneys that underwent ischemic injury, we costained kidney sections with anti-p-H3 and anti-α-tubulin to visualize the mitotic spindle. As an additional spindle marker, we included γ-tubulin that localizes predominantly to the centrosomal region, in our analysis. Depending on whether individual kidney tubules are cut along their longitudinal axis or cross-sectional plane, two different types of angles can be distinguished. The net angle is defined by the relative directions of the mitotic spindle and the kidney tubule (Fig. 3A). Immunofluorescence microscopy revealed that deletion of *Vhl* significantly affected the net angle (Fig. 3B). The cross-section angle that describes the deviation of the mitotic spindle from the plane perpendicular to the apical-basal axis (Fig 3C) was, likewise, affected by *Vhl* deletion (Fig. 3D). Quantification of these immunofluorescence images corroborated that pVHL is a major suppressor of both net and cross-section spindle angle changes *in vivo* (Fig. 3E, F, respectively). The outcome of this analysis was not affected by using either α or γ tubulin as markers for marking the entire spindle and its poles, respectively (Supplemental Fig. 4A). Since in our conditional knockout model, Cre expression is confined to distal but not proximal tubule cells, we compared the effect of *Vhl* deletion on spindle angles in both tubule types. As marker proteins for these cell types, we used Glut1 positivity as a readout for successful *Vhl* knockout in $Vhl^{\Delta/\Delta}$ kidneys and the distal tubule marker

thiazide-sensitive sodium chloride cotransporter (NCC) in Cre-negative kidneys (Supplemental Fig. 4B, C). Importantly, changes in both the net and cross section spindle angles occurred preferentially in distal kidney tubule cells of $Vhl^{\Delta/\Delta}$ mice (Fig. 3G, H). These data suggest that loss of pVHL influences the orientation of cell division within the kidney tissue and argue for a critical function for pVHL in the suppression of mitotic spindle misorientation *in vivo*.

Vhl deletion prompts chromosome missegregation and aneuploidy in injury-exposed kidney epithelial cells

We next asked whether kidney tubule cells lacking *Vhl* and challenged by ischemia would, unlike their Cre-negative littermates, display increased chromosome segregation errors and aneuploidy. To address this, we quantified the frequency of chromosome missegregations in clamped Cre-negative and $Vhl^{\Delta/\Delta}$ kidneys using p-H3 as marker for kidney tubule cells in late anaphase or early telophase. In analogy to the *in vitro* experiments in primary kidney cells, we analyzed the occurrence of lagging chromosomes (single or multiple) and chromosome bridges (Supplemental Fig. 5A). The former allowed estimating the rate of newly generated aneuploidy, while the latter served as internal control. Quantification of these errors in tubule cells revealed that genetic deletion of *Vhl* increased the frequency of lagging chromosomes without affecting the rate of chromosome bridges analyzed in the same samples (Fig. 4A). Analysis of this phenomenon separately in distal and proximal tubules, revealed, like before for spindle misorientation, a selective increase in the percentage of lagging chromosomes in $Vhl^{-/-}$ distal

(but not proximal) tubule cells (Fig. 4B), suggesting that this effect on chromosome missegregation is pVHL-specific. Together, these results support the interpretation that *Vhl* loss impairs the mitotic checkpoint thereby increases the chance that cells with unattached chromosomes undergo cell division.

To examine whether kidney-specific *Vhl* loss results in an aneuploid phenotype, as the increased percentage of lagging chromosomes would suggest, we performed fluorescence in situ hybridization (FISH) with a probe against chromosome 7 on kidney sections from clamped mice. Indeed, as shown in Fig. 4C, *Vhl* deletion caused a considerable number of cells with abnormal copy numbers. Quantitative analysis of chromosome copy numbers per nucleus revealed that the relative frequency of nuclei differing from chromosome 7 disomy was in fact significantly increased in $Vhl^{\Delta/\Delta}$ mice (Fig. 4D). Discrimination between proximal and distal tubule cells further supported the pVHL-specificity of this phenomenon, since the relative frequency of nuclei with a copy number deviating from two was increased specifically in distal tubules of kidney-specific *Vhl* knockout mice (Fig. 4E). These data suggest that distal tubule cells of the kidney lacking *Vhl* are prone to chromosome segregation errors and aneuploidy when challenged to commit to mitotic cell divisions by short-term ischemic injury.

Development of ccRCC precursor lesions following recovery of *Vhl*$^{\Delta/\Delta}$ kidneys from injury

To assess possible long-term effects of kidney injury as a function of pVHL status, we kept *Vhl*$^{\Delta/\Delta}$ and corresponding Cre-negative littermates for 4 months after the injury and analyzed then potential morphological changes of the kidney. Importantly, analysis of hematoxylin and eosin (H&E) stainings of sections derived from clamped and contralateral kidneys of Cre-negative animals did not reveal any histological differences, demonstrating that the ischemia-induced damage is reversible in control animals (Fig. 5A). In contrast to Cre-negative animals, clamped *Vhl*$^{\Delta/\Delta}$ kidneys displayed three major categories of morphological alterations. These included the appearance of dysplastic spots with multilayered tubules and nuclear crowding, clear cells, and simple tubular cysts (Fig. 5B-E). Quantification of the number of spots of each aberration type per kidney section revealed that clamping significantly increased the relative frequency and extend of the aberrations in *Vhl*$^{\Delta/\Delta}$ kidneys, while Cre-negative mice hardly showed any defects both in clamped and unclamped kidneys (Fig. 5F-H). Analysis of proliferation by Ki-67 revealed a moderate increase of basal proliferation in clamped and to a lesser extend in non-clamped *Vhl*$^{\Delta/\Delta}$ kidneys compared to control conditions, while the apoptotic rate remained unchanged (Supplemental Fig. 6A, B). In parallel, also a loss of distal tubule polarity, as evidenced by E-cadherin and atypical protein kinase C (aPKCz) staining was detectable, in particular in the dysplastic spots of clamped *Vhl*$^{\Delta/\Delta}$ kidneys (Fig. 5I, J). These results indicate that the stimuli induced by kidney clamp surgery are able to accelerate the

occurrence of lesions widely believed to constitute precursors of human ccRCC.

Discussion

In this study, we have employed an ischemic kidney regeneration model to unveil potential functions of pVHL in orderly mitotic progression *in vivo*. Our data show that *Vhl* nullizygosity in renal epithelial cells results in spindle misorientation and chromosome missegregation.

We show that 4 months after kidney injury, *Vhl* loss caused changes in the mouse renal epithelium leading to localized dysplasia with multilayered tubules and nuclear crowding, nodules with cytoplasmic clearing, simple tubular cysts, and regions of aberrant polarity. Small nodules with clear cells, and cysts represent likely contributors to key aspects of *VHL*-associated pathology (5, 22-24). The very small spots with clear cells are similar to changes observed in humans with VHL disease (25). In addition, such patients also develop multiple small cysts, similar to those seen in our in $Vhl^{\Delta/\Delta}$ mice. Recently, such lesions have been shown to have lost the *VHL* locus in the cyst-lining cells (26). In line with this, a serial computed tomography (CT) study of patients with *VHL* disease, manifested that cystic lesion precede solid tumor forms during disease progression (24). Intriguingly, we also observed dysplastic spots with multilayered tubules and nuclear crowding in close proximity to the nodules with cytoplasmic clearing, and tubular cysts. Such dysplastic spots may represent very early forms of complex renal cystic epithelium described in humans with VHL disease (27).

Although a direct relationship between the observed mitotic alterations and the development of dysplasia, tubular cysts, and clear cells cannot be assumed, multiple observations suggest that spindle misorientation and chromosome instability constitute tumor-initiating events that may manifest themselves in these phenotypes. An immediate consequence of the observed increase in spindle angles in *Vhl*-deleted cells is likely to be misoriented cell division. During kidney development, the cell division axis of the proliferating tubular epithelial cells is oriented along the tubular axis allowing for an orderly lengthening of the tube (8). Consequently, changes in the direction of cell division might well contribute to loss of regular tissue organization and a kidney tubule widening, ultimately facilitating dysplasia and cyst formation. Previous work has linked the suppression of spindle misorientation by pVHL to its microtubule stabilization function (4, 28). This function is also related to the acknowledged role of pVHL in maintaining the primary cilium (16) and has been proposed as one mechanism for cyst formation when disrupted (13). Given the results presented here, the cystic and dysplastic phenotype, that is a characteristic feature of *VHL*-associated renal pathology, might be the result of both unscheduled cilia resorption and misoriented cell division. The suppression of both of these processes represents core HIF-independent functions of pVHL through microtubule stabilization.

Chromosome missegregation errors were abundantly detected in *Vhl*-deficient renal epithelial cells 5.5 days after ischemic injury. That they were specifically emerging in the distal tubular cells is consistent with the fact that in this model Cre-recombinase is active in this subset of tubular cells, implying that suppression of chromosomal instability is a relevant tumor suppression

function of *Vhl in vivo*. In cultured mammalian cells, pVHL inactivation has been associated with a weakened mitotic checkpoint due to pVHL-loss-of-function mediated downregulation of the Mad2 mitotic checkpoint protein. Lowering levels of Mad2 without eliminating it entirely, provides a potential means of perturbing the mitotic checkpoint in a manner that is compatible with cell survival, but results in a multi-organ tumor phenotype (29). Given that loss of *VHL* is considered an early event in the development of ccRCC, the initiation of a program of chromosomal instability would enforce the occurrence of further aberrations in the face of increased cell proliferation. In this regard, mutations in genes whose products promote aberrant cell proliferation are frequently observed in ccRCC and include components of the PI3K pathway (6). Irrespective, aneuploidy contributes to tumor development in a stochastic manner. This phenomenon could explain the patch-like occurrence of aberrant spots that we observed in clamped $Vhl^{\Delta/\Delta}$ kidneys after four months. This stochastic behavior could also be reflected in the intratumor heterogeneity observed in ccRCC (6, 30).

Acknowledgements The authors would like to thank Dennis Mollenhauer for help with mouse handling and Heather Flynn Gilmer and Patricia T. Greipp (Medical Genome Facility, Mayo Clinics, Cleveland, U.S.A) for technical assistance with FISH probes. M.P.H. and M.D. like to acknowledge the Zurich Life Science PhD program. M.P.H. was supported as a Boehringer Ingelheim Fonds (BIF) PhD fellow. W. K. is supported by a grant from the Swiss National Science Foundation and the SwissBRIDGE Cancer Award.

References

1. Kaelin WG. Von Hippel-Lindau disease. Annual review of pathology. 2007;2:145-73.
2. Frew IJ, Krek W. pVHL: a multipurpose adaptor protein. Sci Signal. 2008;1:pe30.
3. Li M, Kim WY. Two sides to every story: the HIF-dependent and HIF-independent functions of pVHL. Journal of cellular and molecular medicine. 2011;15:187-95.
4. Thoma CR, Toso A, Gutbrodt KL, Reggi SP, Frew IJ, Schraml P, et al. VHL loss causes spindle misorientation and chromosome instability. Nat Cell Biol. 2009;11:994-1001.
5. Van Poppel H, Nilsson S, Algaba F, Bergerheim U, Dal Cin P, Fleming S, et al. Precancerous lesions in the kidney. Scand J Urol Nephrol Suppl. 2000:136-65.
6. Creighton CJ, Morgan M, Gunaratne PH, Wheeler DA, Gibbs RA, Gordon Robertson A, et al. Comprehensive molecular characterization of clear cell renal cell carcinoma. Nature. 2013.
7. Patel V, Li L, Cobo-Stark P, Shao X, Somlo S, Lin F, et al. Acute kidney injury and aberrant planar cell polarity induce cyst formation in mice lacking renal cilia. Hum Mol Genet. 2008;17:1578-90.
8. Fischer E, Legue E, Doyen A, Nato F, Nicolas JF, Torres V, et al. Defective planar cell polarity in polycystic kidney disease. Nat Genet. 2006;38:21-3.
9. Hanahan D, Weinberg RA. Hallmarks of cancer: the next generation. Cell. 2011;144:646-74.
10. Sotillo R, Schvartzman JM, Socci ND, Benezra R. Mad2-induced chromosome instability leads to lung tumour relapse after oncogene withdrawal. Nature. 2010.
11. Humphreys BD, Valerius MT, Kobayashi A, Mugford JW, Soeung S, Duffield JS, et al. Intrinsic epithelial cells repair the kidney after injury. Cell Stem Cell. 2008;2:284-91.
12. Kennedy SE, Erlich JH. Murine renal ischaemia-reperfusion injury. Nephrology (Carlton). 2008;13:390-6.
13. Frew IJ, Thoma CR, Georgiev S, Minola A, Hitz M, Montani M, et al. pVHL and PTEN tumour suppressor proteins cooperatively suppress kidney cyst formation. EMBO J. 2008;27:1747-57.
14. Shao X, Somlo S, Igarashi P. Epithelial-specific Cre/lox recombination in the developing kidney and genitourinary tract. J Am Soc Nephrol. 2002;13:1837-46.
15. Albers J, Rajski M, Schonenberger D, Harlander S, Schraml P, von Teichman A, et al. Combined mutation of Vhl and Trp53 causes renal cysts and tumours in mice. EMBO molecular medicine. 2013.
16. Thoma CR, Frew IJ, Hoerner CR, Montani M, Moch H, Krek W. pVHL and GSK3beta are components of a primary cilium-maintenance signalling network. Nat Cell Biol. 2007;9:588-95.
17. Ricke RM, Jeganathan KB, Malureanu L, Harrison AM, van Deursen JM. Bub1 kinase activity drives error correction and mitotic checkpoint control but not tumor suppression. J Cell Biol. 2012;199:931-49.
18. Mood AM. On the Asymptotic Efficiency of Certain Nonparametric Two-Sample Tests. The Annals of Mathematical Statistics. 1954;25:514-22.

19. R Development Core Team. R: A language and environment for statistical computing. In: Computing RFfS, editor. Vienna, Austria: R Development Core Team; 2008.
20. Maxwell PH, Wiesener MS, Chang GW, Clifford SC, Vaux EC, Cockman ME, et al. The tumour suppressor protein VHL targets hypoxia-inducible factors for oxygen-dependent proteolysis. Nature. 1999;399:271-5.
21. Zelzer E, Levy Y, Kahana C, Shilo BZ, Rubinstein M, Cohen B. Insulin induces transcription of target genes through the hypoxia-inducible factor HIF-1alpha/ARNT. EMBO J. 1998;17:5085-94.
22. Salome F, Colombeau P, Fermeaux V, Cazaux P, Dumas JP, Pfeifer P, et al. Renal lesions in Von Hippel-Lindau disease: the benign, the malignant, the unknown. Eur Urol. 1998;34:383-92.
23. Mandriota SJ, Turner KJ, Davies DR, Murray PG, Morgan NV, Sowter HM, et al. HIF activation identifies early lesions in VHL kidneys: evidence for site-specific tumor suppressor function in the nephron. Cancer Cell. 2002;1:459-68.
24. Choyke PL, Glenn GM, Walther MM, Zbar B, Weiss GH, Alexander RB, et al. The natural history of renal lesions in von Hippel-Lindau disease: a serial CT study in 28 patients. AJR American journal of roentgenology. 1992;159:1229-34.
25. Rini BI, Campbell SC, Escudier B. Renal cell carcinoma. Lancet. 2009;373:1119-32.
26. Montani M, Heinimann K, von Teichman A, Rudolph T, Perren A, Moch H. VHL-gene deletion in single renal tubular epithelial cells and renal tubular cysts: further evidence for a cyst-dependent progression pathway of clear cell renal carcinoma in von Hippel-Lindau disease. The American journal of surgical pathology. 2010;34:806-15.
27. Bausch B, Jilg C, Glasker S, Vortmeyer A, Lutzen N, Anton A, et al. Renal cancer in von Hippel-Lindau disease and related syndromes. Nature reviews Nephrology. 2013;9:529-38.
28. Thoma CR, Matov A, Gutbrodt KL, Hoerner CR, Smole Z, Krek W, et al. Quantitative image analysis identifies pVHL as a key regulator of microtubule dynamic instability. J Cell Biol. 2010;190:991-1003.
29. Michel LS, Liberal V, Chatterjee A, Kirchwegger R, Pasche B, Gerald W, et al. MAD2 haplo-insufficiency causes premature anaphase and chromosome instability in mammalian cells. Nature. 2001;409:355-9.
30. Gerlinger M, Rowan AJ, Horswell S, Larkin J, Endesfelder D, Gronroos E, et al. Intratumor heterogeneity and branched evolution revealed by multiregion sequencing. N Engl J Med. 2012;366:883-92.

Figure Legends

Figure 1: Increased chromosome missegregation and spindle misorientation in mouse primary renal epithelial cells (MRECs) upon genetic loss of *Vhl*. A, Western blot analysis of MRECs isolated from $Vhl^{fl/fl}$ mice after genetic elimination of Vhl through adenoviral delivery of Cre-recombinase (AdCre). LacZ serves as control (AdLacZ). B, Example images of chromosome segregation errors. Chromosomes visualized by DAPI, α-tubulin in green (scale bar: 10 µm). C, Quantification of frequency of segregation errors defined in B, n = 81 (AdLacZ), 82 (AdCre) [lagg.: lagging, chrom.: chromosome, mult.: multiple (n ≥ 2), two categorical (lagging vs. rest) χ^2 test]. D, Assessment of chromosome numbers from metaphase spreads; n = 36 (AdLacZ), n = 38 (AdCre). E, The spindle angle, α, is defined by the given formula. d: spindle diameter, z: distance between spindle poles in a plane perpendicular to the support. F, Representative Z-stack images demonstrating the spindle pole orientation (stained by gamma-tubulin in red) in AdCre or AdLacZ infected cells. Scale bar: 5 µm, counterstained with DAPI (blue). G, Quantification of spindle angle upon Cre recombinase mediated Vhl inactivation (AdLacZ n = 44, AdCre n = 33; line indicates median, Mann Whitney U test). H, Measurement of spindle diameter (mean ± stdev, µm).

Figure 2: Kidney injury induces proliferative and apoptotic response independently of pVHL status. A, Timeline of the renal injury experiment. B, Quantification of the post-injury kidney weight for Cre- and $Vhl^{\Delta/\Delta}$ mice; both clamped and control kidneys included (n = 4 mice per genotype, mean ± stdev). C, Representative images showing proliferative response by

phosphorylated histone 3 (p-H3, green) and Ki-67 (red) in kidneys of Cre- and $Vhl^{\Delta/\Delta}$ mice following renal injury (counterstained with DAPI, scale bar: 50 µm). D, Quantification of Ki-67 staining in Cre- and $Vhl^{\Delta/\Delta}$ mice 5.5 days post-injury (n = 14 independent slides per genotype, mean ± SEM, Student's *t*-test). E, Quantification of p-H3 staining in Cre- and $Vhl^{\Delta/\Delta}$ mice post-injury (n = 7 independent slides per genotype, mean ± SEM, Student's *t*-test). F, Assessment of apoptotic nuclei (red) by terminal deoxynucleotidyl transferase dUTP nick end labeling (TUNEL) assay in clamped kidneys, scale bar: 20 µm. G, Quantification of TUNEL staining in Cre- and $Vhl^{\Delta/\Delta}$ mice post-injury (n = 7 independent slides per genotype, mean ± SEM, Student's *t*-test).

Figure 3: *Vhl* deletion induces spindle misorientation in distal kidney tubules. A, Schematic representation of the net spindle angle (α) calculation: a refers to the direction of kidney tubule, while b refers to the spindle position. Dotted lines are located inside the tubules. B, Images of longitudinal tubule kidney sections stained with antibodies against α-tubulin (red) and phosphorylated histone 3 (p-H3, green) and counterstained with DAPI (blue) representing the spindle orientation in Cre- and $Vhl^{\Delta/\Delta}$ kidneys 5.5 days after ischemic injury (scale bar: 20 µm). Thick lines represent the direction of the kidney tubule while thin lines indicate the spindle orientation. Inserts: enlargement of mitotic spindle. Top/bottom: relative z stack position. C, Schematic representation of the cross-section spindle angle (α) calculation: a refers to the plane perpendicular to apical-basal polarity axis, b describes the position of mitotic spindle. D, Example pictures showing spindle orientation in cross-sections of kidney tubules treated as in B. E, Distribution

of the net spindle angle (n = 64 for Cre- and n = 74 for *Vhl*$^{\Delta/\Delta}$). F, Same as E but for cross-section angle (n = 56 for Cre- and n = 42 for *Vhl*$^{\Delta/\Delta}$). G, Quantification of the net spindle angle with respect to proximal and distal tubules (bar indicates median, n = 4 mice per genotype, Mann-Whitney U test). H, Same as G but for cross-section angle.

Figure 4: Chromosome instability and aneuploidy is instigated specifically in Vhl-/- distal tubules following kidney injury. A, Relative frequency of lagging chromosomes (single or multiple) and chromosome bridges in tubules of clamped kidneys 5.5d post surgery (n = 4 mice per genotype, n = 180 (Cre-), n = 138 (*Vhl*$^{\Delta/\Delta}$), χ^2 test). B, Quantification of segregation errors in distal and proximal tubules (Cre-: n = 21 (dist.), n = 45 (prox.), *Vhl*$^{\Delta/\Delta}$: n = 35 (dist.), n = 36 (prox.)). C, Exemplary pictures of chromosome 7 fluorescence in situ hybridisation (FISH, orange), scale bar: 20 µm. D, Distribution of chromosome 7 copy numbers determined by FISH (n = 3 mice per genotype, n > 250 nuclei; Mood test). E, Relative distribution of disomic vs. non-disomic nuclei (based on chromosome 7) in distal and proximal tubules. (n = 3 mice per genotype, n > 500 nuclei; χ^2 test).

Figure 5: *Vhl*$^{\Delta/\Delta}$ mice develop ccRCC-precursor lesions 4 months post-injury. A, Representative hematoxylin & eosin (H&E) staining of clamped and non-clamped kidneys from Cre-negative animals 4 months post surgery; scale bar: 50 µm. B, Same as A, but for *Vhl*$^{\Delta/\Delta}$ mice. C, H&E staining of dysplastic spot (arrow) in clamped *Vhl*$^{\Delta/\Delta}$ kidney; scale bar: 20 µm. D, H&E staining of

clear cells (arrow) in clamped *Vhl*$^{\Delta/\Delta}$ kidney; scale bar: 20 μm. E, H&E staining of cyst (arrow) in clamped *Vhl*$^{\Delta/\Delta}$ kidney; scale bar: 20 μm. F, Quantification of the dysplastic spots frequency per kidney section (normalized to relative area, localized: ≈ 50 μm^2, extended: >> 50 μm^2, n = 4 mice per genotype, Student's *t*-test with both categories combined). G, Quantification of clear cells frequency per kidney section (normalized to relative area, n = 4 mice per genotype, Student's *t*-test with both categories combined). H, Quantification of tubular cysts frequency per kidney section (normalized to relative area, small: ≈ 1 tubule diameter, large: >> 1 tubule diameter, n = 4 mice per genotype, Student's *t*-test). I, Aberrant E-cadherin (green) staining in *Vhl*$^{\Delta/\Delta}$ mice that underwent ischemic injury compared to operated Cre-negative mice; DBA (yellow): distal tubule marker, DAPI in blue. J, Aberrant aPKCz staining (red) in *Vhl*$^{\Delta/\Delta}$ mice that underwent ischemic injury compared to operated Cre- mice; NCC (yellow): distal tubule marker, Glut1 (yellow): *Vhl* knockout marker, DAPI in blue; scale bar: 20 μm.

Author Manuscript Published OnlineFirst on December 20, 2013; DOI: 10.1158/0008-5472.CAN-13-2040
Author manuscripts have been peer reviewed and accepted for publication but have not yet been edited.

Hell+Duda_Fig1

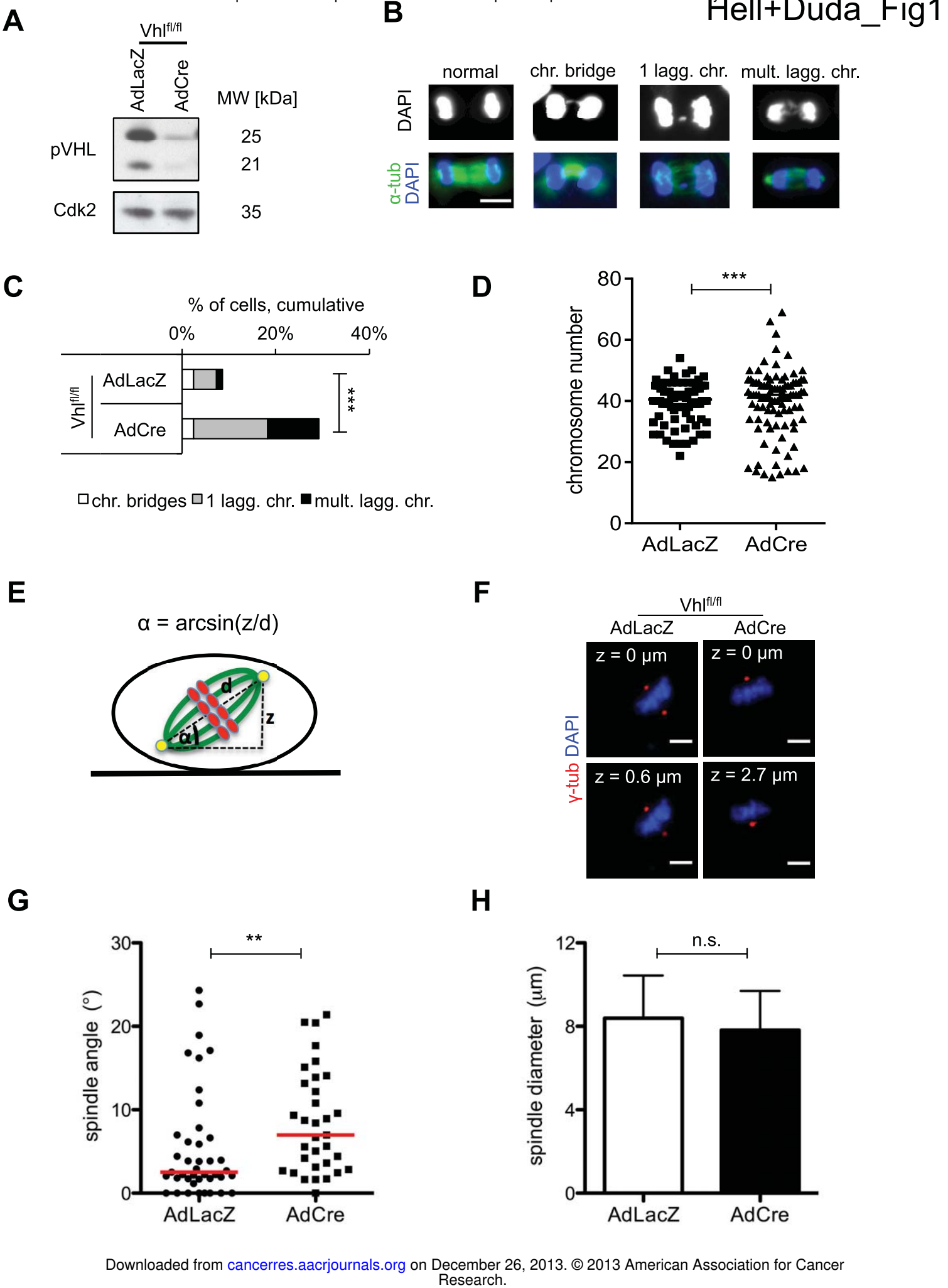

Author Manuscript Published OnlineFirst on December 20, 2013; DOI: 10.1158/0008-5472.CAN-13-2040
Author manuscripts have been peer reviewed and accepted for publication but have not yet been edited.

Hell+Duda_Fig2

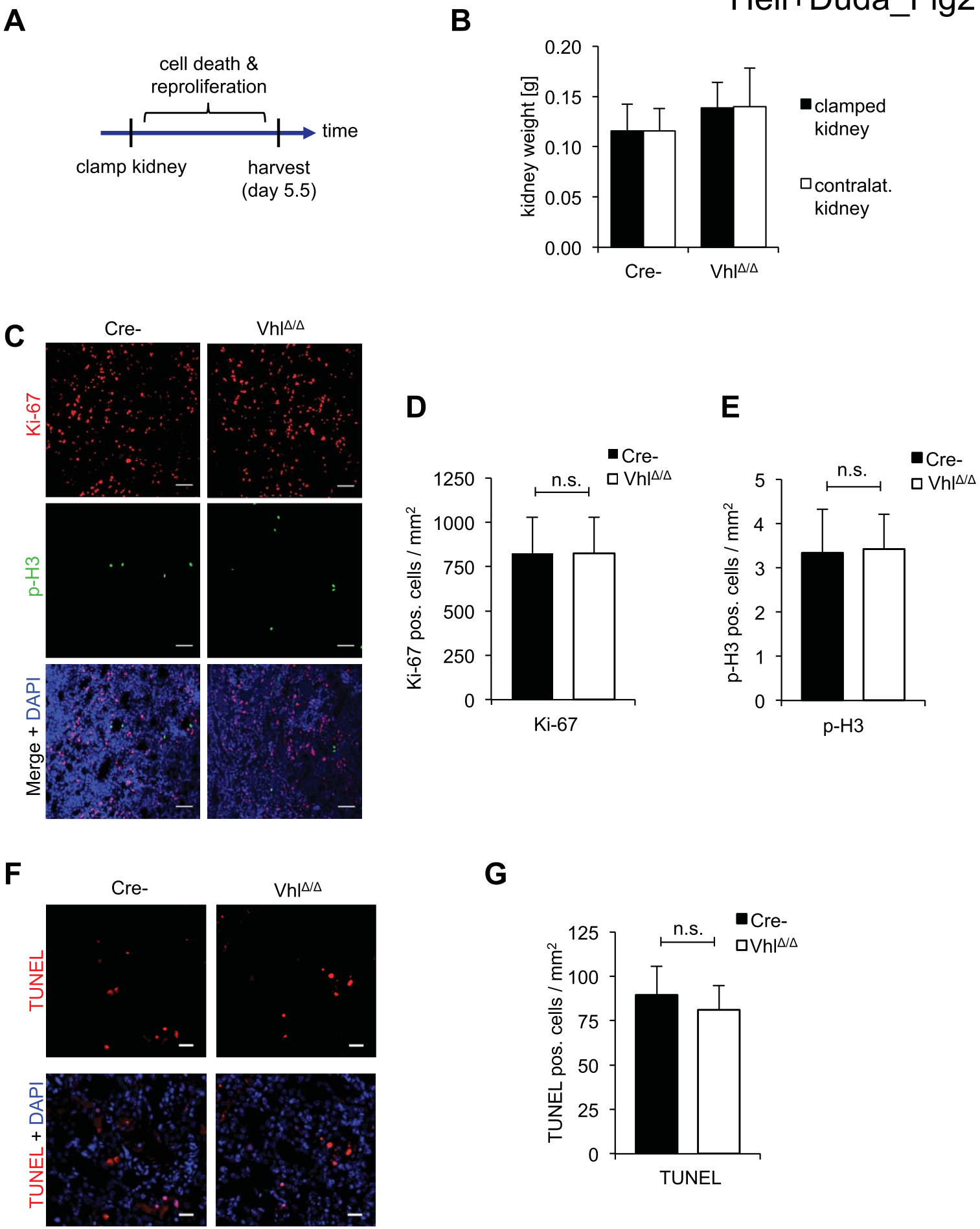

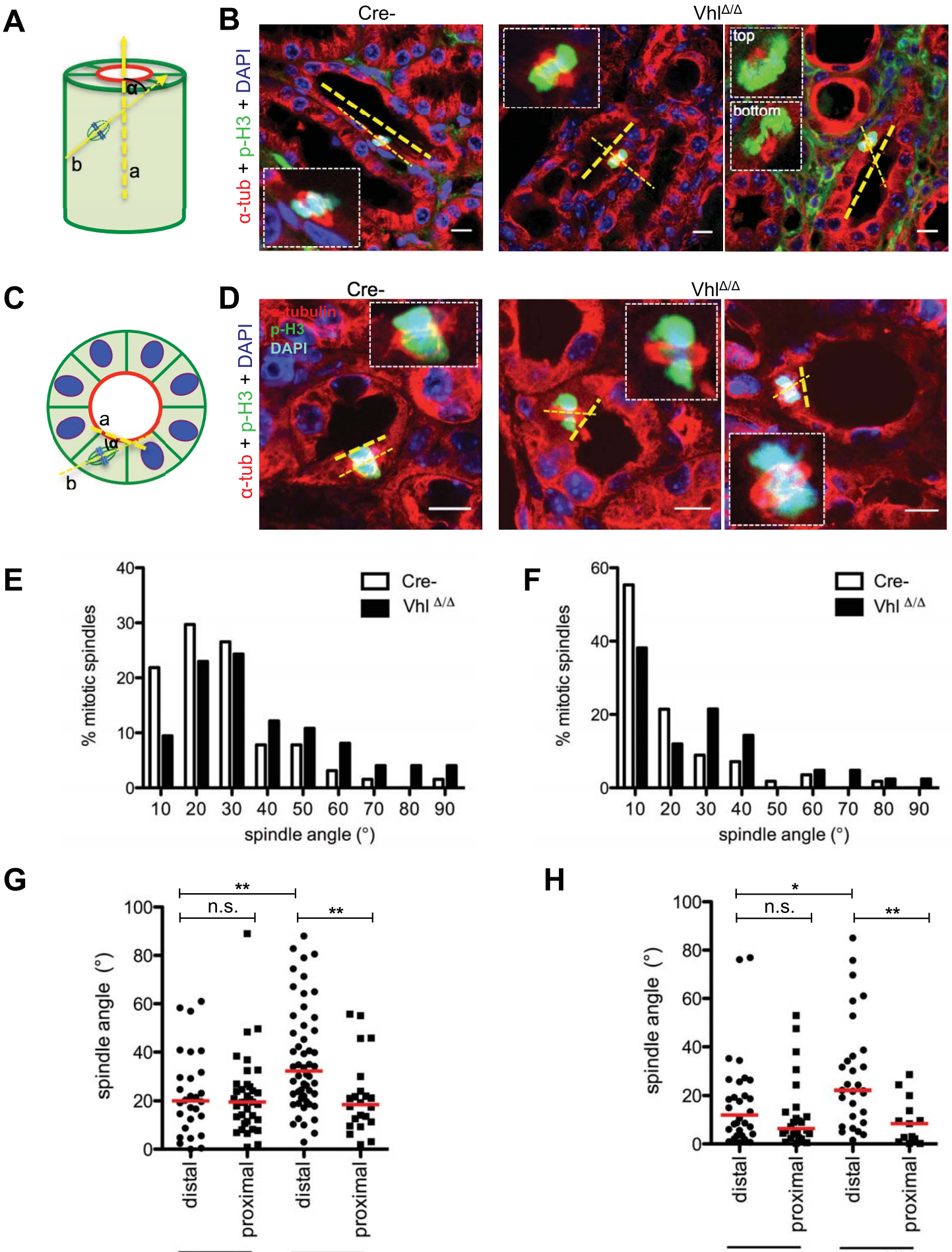

Author Manuscript Published OnlineFirst on December 20, 2013; DOI: 10.1158/0008-5472.CAN-13-2040
Author manuscripts have been peer reviewed and accepted for publication but have not yet been edited.

Hell+Duda_Fig4

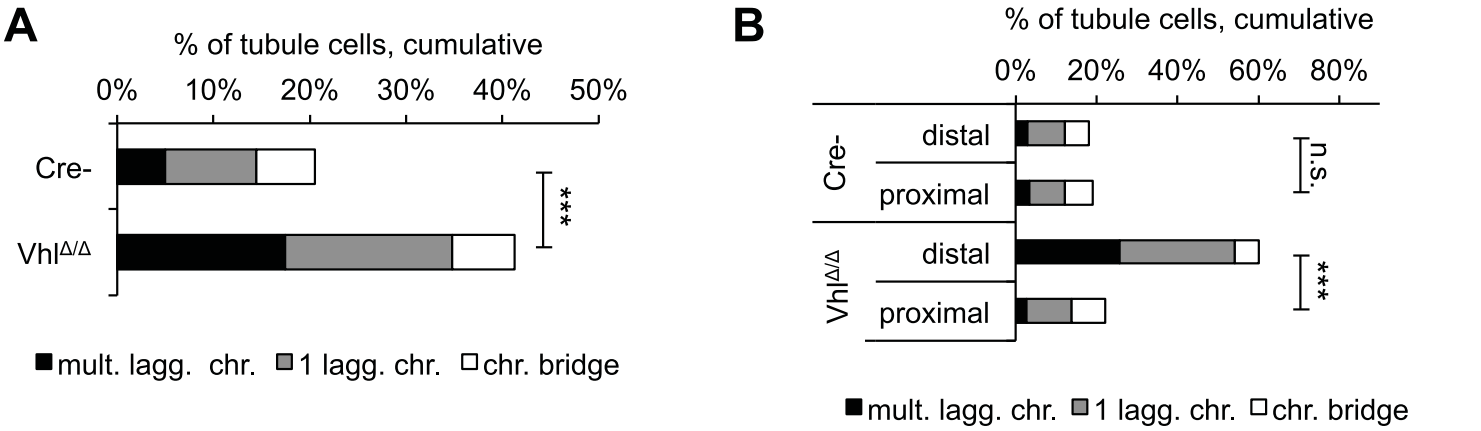

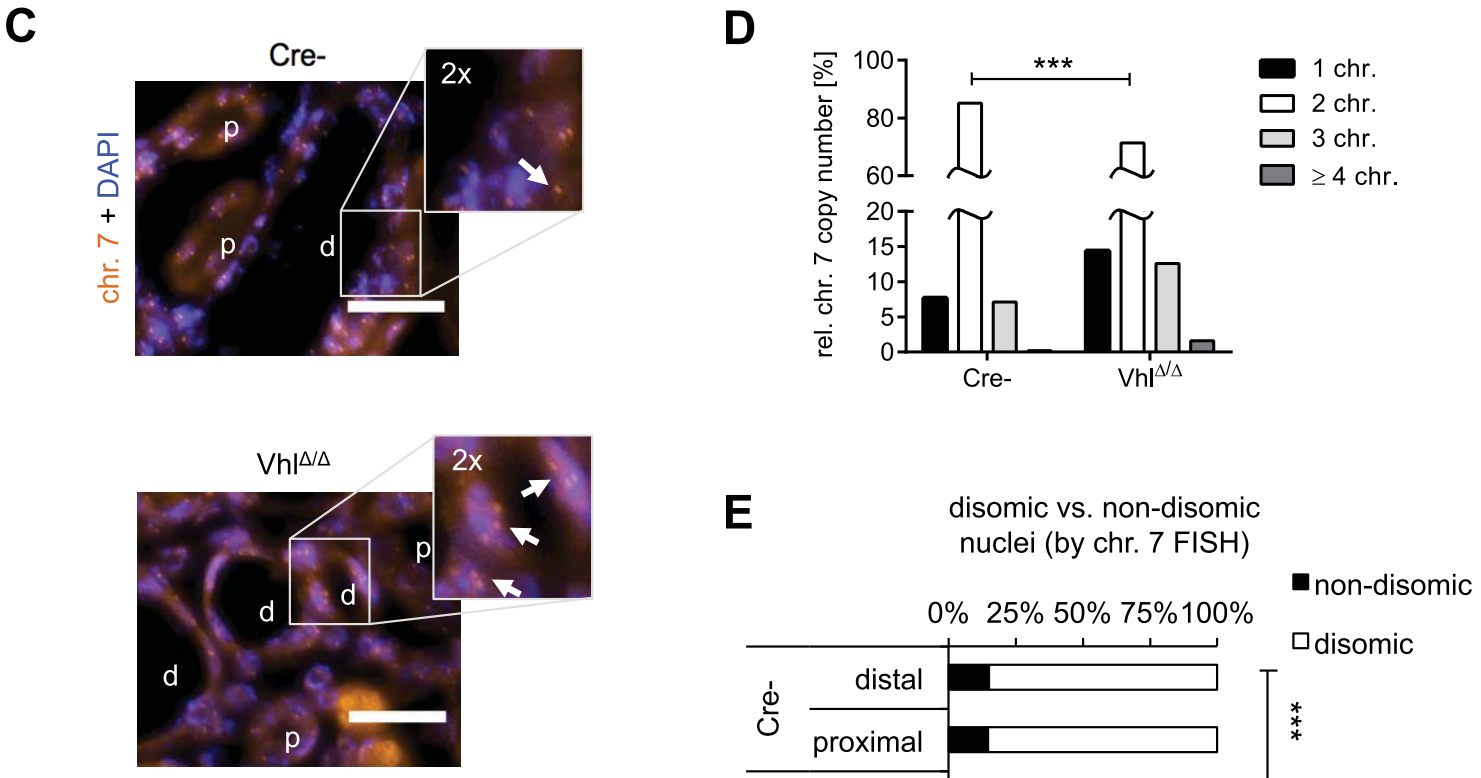

Author Manuscript Published OnlineFirst on December 20, 2013; DOI: 10.1158/0008-5472.CAN-13-2040
Author manuscripts have been peer reviewed and accepted for publication but have not yet been edited.

Hell+Duda_Fig5